Editors' Suggestion

Arousal tunes neuronal avalanches across a directed percolation critical point

Brandon R. Munn [1,2,*] Christopher Whyte [2] Eli J. Müller [1,2] and James M. Shine [2]
[1]*School of Physics, Faculty of Science, The University of Sydney, Sydney, New South Wales, Australia*
[2]*School of Medical Science, Faculty of Medicine and Health, The University of Sydney, Sydney, New South Wales, Australia*

(Received 22 October 2025; accepted 5 June 2026; published 18 August 2026)

Neuromodulatory levels in the brain change moment to moment, yet are typically ignored in studies of neural criticality, where empirical support remains varied. Here we show in a biophysical network of bursting neurons that arousal acts as a mechanistic control parameter for a directed percolation phase transition. At intermediate arousal, neuronal activity exhibits peaked susceptibility, power-law avalanche size and duration distributions, universal shape collapse, and anomalous diffusion, jointly satisfying the hyperscaling relation of the 2+1-dimensional directed percolation universality class. Reanalyzing extracellular recordings in awake mice, we find that time-resolved susceptibility tracks pupil-inferred arousal as the model predicts. These results identify arousal as a physiological control parameter for neural criticality, offering a statistical-physics basis for the Yerkes-Dodson effect, and imply that arousal should be tracked at fine temporal resolution to obtain reliable empirical estimates of neural criticality.

DOI: 10.1103/xby9-6mtn

I. INTRODUCTION

The coordination of neuronal activity across spatiotemporal scales exhibits signatures consistent with criticality, including heavy-tailed avalanche statistics and long-range correlations [1–6]. Whether the brain operates near criticality remains a contested empirical question, with evidence varying substantially across species, preparations, and behavioral states [6,7]. We argue that a major source of this heterogeneity is the ascending arousal system, which is ideally placed to act as a controller of critical order [8–11].

From a functional perspective, maintaining a fixed critical point is neither biologically plausible, given the rich neural heterogeneity and dynamic biophysical properties, nor adaptive. Different dynamical regimes offer distinct computational benefits: the critical point confers maximal susceptibility and dynamic range [12,13], subcritical dynamics enhance specificity and noise-resistant processing [14], and transient supercriticality promotes exploration of neural state space. Brains, therefore, likely dynamically regulate their proximity to a critical point in a context-dependent manner [15]. Indeed, neural systems can flexibly adjust sensitivity across many orders of magnitude, from detecting single photons to selectively filtering relevant signals amid a cacophony of noise (cocktail party effect), implying the existence of physiological mechanisms that tune network dynamics across regimes on behaviorally relevant timescales.

Through subcortical neuromodulatory pathways, such as the noradrenergic and diffuse matrix thalamic projections [Fig. 1(a)], the arousal system regulates neural state (wake-sleep) and adaptation to stimuli [16–18] and exhibits an inverted-U relationship with cognitive performance known as the Yerkes-Dodson law [19–22]. A key mechanism controlled by the arousal system is the probabilistic transition in pyramidal cells from tonic spiking [Fig. 1(b), green] to burst firing [clusters of high-frequency spiking; Fig. 1(b), orange] by coupling the electrotonically separated soma and apical dendrites [23]. Bursting enhances synaptic reliability and has been argued to implement a tertiary neural code [24] that integrates top-down and bottom-up processing [25]. Bursting is a conserved and functionally relevant feature, yet its spatiotemporal dynamical role remains largely unknown.

Here we show that arousal-controlled bursting can serve as a control parameter for a directed percolation (DP) phase transition. DP is the canonical universality class for nonequilibrium continuous phase transitions in systems with a unique absorbing state [26], yet a complete demonstration of DP scaling has remained elusive in neural systems, as studies typically report size and duration avalanche exponents [27–29] but not spatial diffusion scaling, which is required to satisfy the DP hyperscaling relation. Using a network of nonlinear neurons, we demonstrate that increasing the likelihood of bursting tunes network activity across dynamical phases. At intermediate arousal levels, we observe (1) peaked susceptibility, (2) power-law avalanche size and duration distributions and anomalous diffusion with exponents $(\tau,\ \alpha, z)$ satisfying a complete hyperscaling characterization of 2+1-dimensional DP, and (3) universal avalanche shape collapse. In addition, time-resolved analyses of cortical recordings show that fluctuations in arousal (assessed via pupil area) covary with time-resolved signatures of criticality consistent with our model's predictions. These results identify arousal as a mechanistic control parameter linking cellular physiology to nonequilibrium statistical physics, helping to explain why empirical reports of criticality vary across studies and suggesting how the brain may flexibly mitigate trade-offs of being in a fixed critical state.

II. MODEL

To test whether arousal-controlled bursting regulates critical dynamics, we simulated a spatially embedded network of dual-compartment nonlinear pyramidal neurons [Fig. 1(c)]

*Contact author: brandon.munn@sydney.edu.au

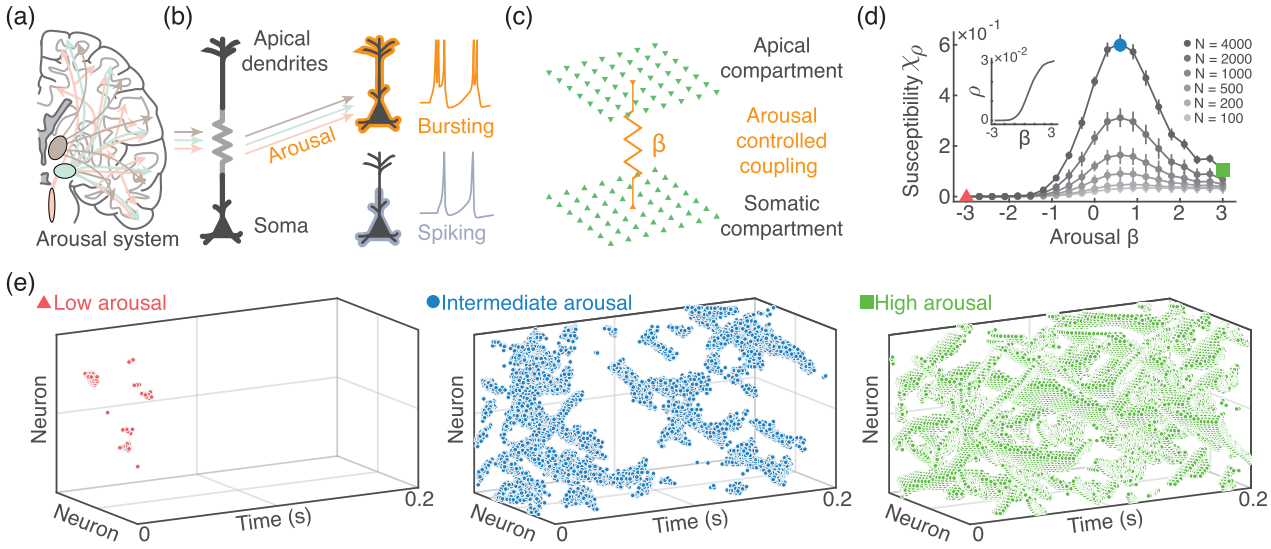

FIG. 1. Arousal acts as a mechanistic control parameter of neural bursting producing rich spatiotemporal patterns and peaked susceptibility at intermediate arousal. (a) The ascending arousal system comprises a distributed set of subcortical nuclei (brainstem, thalamus, forebrain) that modulate cortical state. (b) Arousal regulates the coupling between apical dendrites and soma of pyramidal neurons, promoting transitions from tonic spiking (purple) to high-frequency bursting (yellow). (c) The network model consists of dual-compartment neurons, E:I balanced, toroidal connectivity. The arousal parameter β controls the apical-somatic coupling and resulting burst density (ρ). (d) Susceptibility χ_ρ exhibits an inverted-U profile, peaking at intermediate arousal. The susceptibility peak increases and becomes more pronounced with greater number of sampled neurons (N). Error bars show 95% CI. (e) Example spatiotemporal burst activity for three regimes of arousal: low [left red, square in (d)], intermediate [middle blue; chosen as the peak susceptibility in (d) blue circle], and high arousal [right green, triangle in (d)], showing sparse, spatiotemporally propagating, and dense dynamics, respectively.

[30–32]. Somatic membrane dynamics followed the dimensionless Izhikevich form

$$\frac{dv}{dt} = 0.04v^2 + 5v - u + I, \tag{1}$$

$$\frac{du}{dt} = 0.02(0.2v - u), \tag{2}$$

with after spike reset

$$v \to c(t),\ u \to u + d(t),\ \text{if } v \geqslant 30\ \text{mV},$$

where v is the membrane potential, u is the recovery variable, and I is synaptic and external input [33]. Neurons were arranged on a two-dimensional toroidal grid ($N = 70 \times 70$) with excitatory-inhibitory balanced "Mexican-hat" connectivity (within a radius of 10 units)—short-range excitation surrounded by longer-range inhibition, approximating the canonical receptive-field structure of cortical neurons and supporting traveling waves implicated in cortical processing [34]. The Mexican-hat kernel is a standard effective connectivity that collapses the local E:I:E motif (where excitatory cells drive nearby inhibitory interneurons that mediate lateral inhibition) rather than explicitly simulating inhibitory cells and thus relaxing Dale's principle at the scale of cellular connectivity. This connectivity structure captures the net spatial profile of local excitation and lateral inhibition while preserving population homogeneity, ensuring the emergent spatiotemporal patterns reflect the systems dynamical regime rather than underlying neural heterogeneity. The model is driven with a weak external drive ($\mu = 0, \sigma = 5$ mV), yielding baseline firing rates of ∼3 Hz in the absence of bursting, in line with empirical observations of the cortex at rest.

Arousal was modeled by a gating dendritic compartment that switches the after-spike reset parameters $c(t)$, $d(t)$, from tonic spiking ($c = -65$, $d = 8$) to high-frequency bursting ($c = -55$, $d = 4$), by depolarizing the resting state of the cell (c) and reducing spike-frequency adaptation (d). Crucially, our analysis isolates true bursting generated by apical-somatic coupling from burstiness arising from irregular tonic firing. The arousal parameter β sets the probability that dendritic input will trigger the bursting mode via standardized spatially correlated apical drive ($\sigma = \sqrt{N}$). Somatic and apical input statistics were held fixed across simulations; only β was varied, thereby isolating the dynamical role of arousal-controlled bursting.

III. RESULTS

A. Arousal tunes burst density and susceptibility

We first assessed whether bursting acts as an order parameter for a phase transition. The mean burst density, $\rho_t = 1/N \sum_i \delta_i(t)$, increased smoothly and monotonically with β [Fig. 1(d), inset], with no visible discontinuity consistent with a continuous (second-order) transition. While finite-size simulations cannot rule out a smoothed first-order transition on the bases of order parameter the joint avalanche scaling below identifies the universality class. We found that the dynamic susceptibility

$$\chi_\rho = N\left(\langle \rho_t^2 \rangle - \langle \rho_t \rangle^2\right) \tag{3}$$

exhibited a pronounced maximum at intermediate β, which increased with larger neuronal sampling [N; Fig. 1(d)], suggesting a critical regime [35], and motivating exploration at

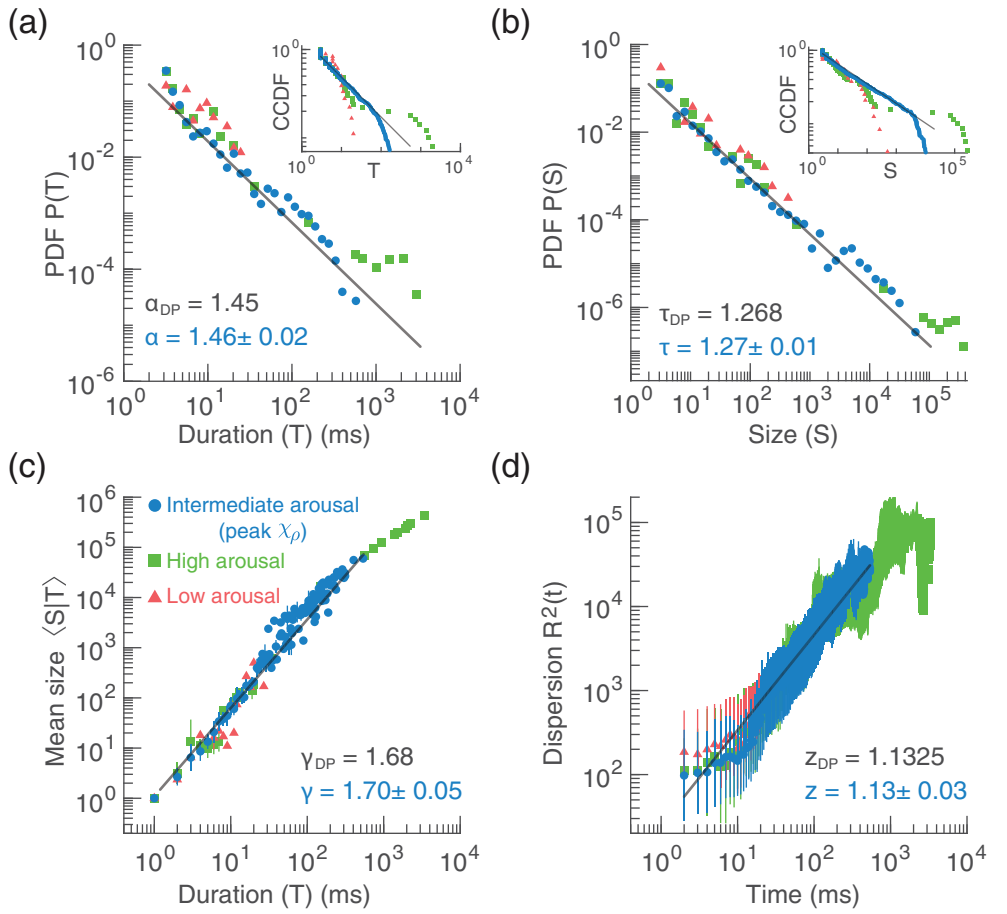

FIG. 2. Critical burst avalanches belong to the 2+1 directed percolation universality class. Burst avalanche size (a) and duration (b) probability density functions (PDFs) for low (red triangles), intermediate (peak susceptibility; blue circles), and high arousal (green squares). Intermediate arousal follows power laws consistent with DP exponents (black lines). Insets show complementary cumulative distribution functions (CCDFs). (c) Mean size to duration scaling $\langle S|T\rangle$. (d) Mean-squared displacement, $R^2(t)$. In (c) and (d), solid lines indicate DP theoretical exponents. Error bars are 95% CI.

[Fig. 1(d), blue circle], below [Fig. 1(d), red triangle], and beyond [Fig. 1(d), green square] this peak.

We demonstrate the underlying burst dynamics supporting this increase in susceptibility by contrasting the spatiotemporal burst activity across three representative regimes: low arousal [Fig. 1(e), red], intermediate arousal at the peak susceptibility [Fig. 1(e), blue], and high arousal [Fig. 1(e), green]. Each arousal regime revealed qualitatively distinct spatiotemporal patterns. At low arousal, bursts were sparse and short-lived; at intermediate arousal, we observed spatiotemporally contiguous burst cascades; at high arousal, bursting was globally synchronous and localized patterns frequently intersected. These patterns resembled percolating clusters observed in nonequilibrium phase transitions.

B. Avalanche scaling and directed percolation hyperscaling

To characterize the propagation of bursts at and around this susceptibility peak, we defined burst avalanches as spatiotemporally contiguous clusters of bursts connected by synaptic causality. This procedure allowed multiple simultaneous avalanches to be tracked over time. Overlapping cascades were resolved by terminating the smaller avalanche at their intersection. The diversity of coexisting cascades also peaked at intermediate β, consistent with maximally heterogeneous dynamics [36].

Static order parameter scaling is notoriously difficult to assess in finite biophysical networks [37]. We therefore characterized criticality through avalanche statistics, size S (total bursts), duration T (active time steps), and their scaling relation $\langle S|T\rangle$, which together provide a robust basis for identifying universality. At criticality, these quantities follow power laws:

$$P(T) \sim T^{-\alpha}, \tag{4}$$

$$P(S) \sim S^{-\tau}, \tag{5}$$

$$\langle S|T\rangle \sim T^{\gamma}. \tag{6}$$

However, while the general framework of neuronal avalanches allows flexibility in these exponents [7]—with avalanche statistics also reported near noise-induced first-order transitions [38]—DP is the canonical universality class for the nonequilibrium continuous phase transition into an

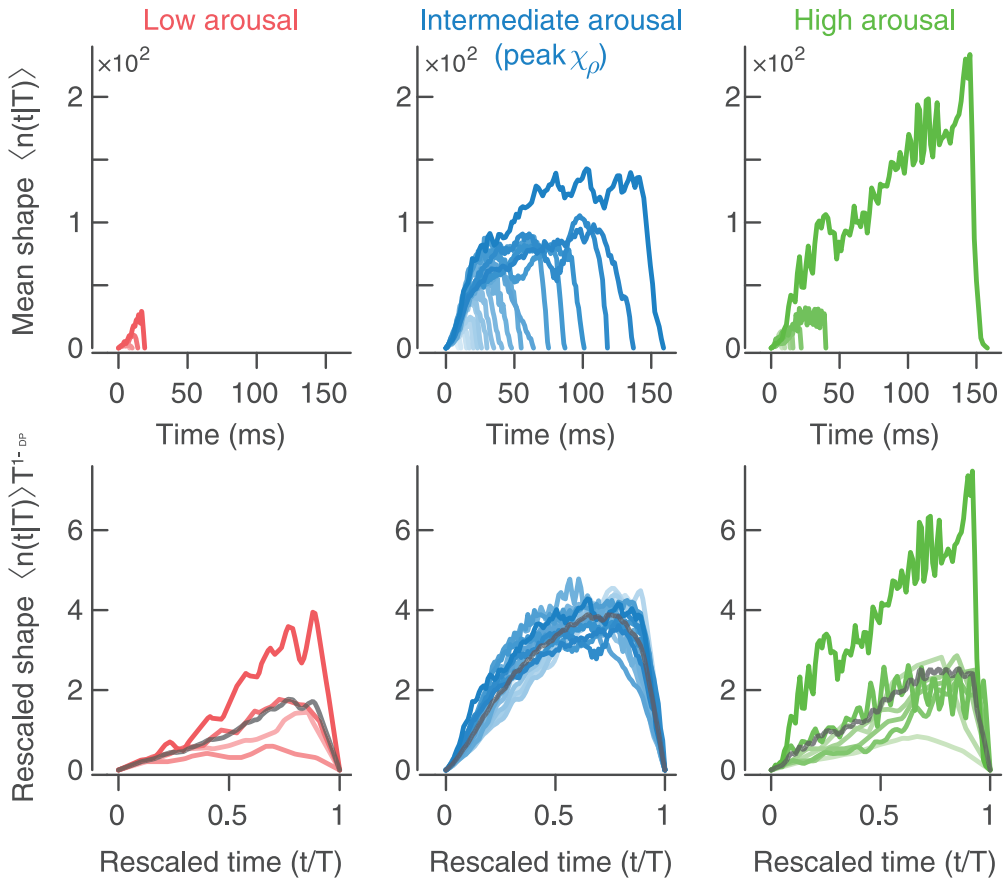

FIG. 3. Avalanche shape collapse. (Top) Mean avalanche profiles $\langle n(t|T)\rangle$ for the three arousal regimes. (Bottom) Rescaled avalanche shapes using the DP-predicted scaling relation γ_{DP} with duration-averaged profile (black line).

absorbing state [26,37]. Crucially, DP requires the joint emergence of both spatial and temporal scaling, and the simultaneous matching of the full hyperscaling exponent set, providing a far more constrained signature than power-law avalanches alone.

To test for DP, we note that DP is fully characterized by the spreading exponents (η, δ, z), which follow

$$N(t) \sim t^{\eta}, \tag{7}$$

$$P_{\mathrm{surv}}(t) \sim t^{-\delta}, \tag{8}$$

$$R^2(t) \sim t^{z}, \tag{9}$$

where $N(t)$ is the number of active sites after t time steps (across both active and quenched avalanches), $P_{\mathrm{surv}}(t)$ is the survival probability, and R^2 is the spatial dispersion R^2 (mean-squared displacement) [26]. In 2+1 dimensions, DP, numerical estimates yield $\eta \approx 0.23$, $\delta \approx 0.45$, $z \approx 1.05$ [1]. From these, the avalanche duration is given by the negative derivative of the survival function,

$$P(T) = -\frac{d}{dT}P_{\mathrm{surv}}(T) \sim T^{-(\delta+1)} \Rightarrow \alpha = \delta + 1. \tag{10}$$

The mean avalanche size, thus, scales as

$$\langle S|T\rangle \approx\sim \int_0^T \frac{N(t)}{P_{\mathrm{surv}}(t)}dt \sim T^{1+\eta+\delta} \Rightarrow \gamma = 1+\eta+\delta. \tag{11}$$

Then, noting the conditional scaling ansatz, $P(S|T) \sim T^{-\gamma}G(\frac{S}{T^{\gamma}})$, and by marginalizing $P(S,T)$, we obtain

$$P(S) = \int P(S|T)P(T)dT \sim S^{-\frac{\gamma+\alpha-1}{\gamma}} \Rightarrow \tau = \frac{1+\eta+2\delta}{1+\eta+\delta}. \tag{12}$$

Thus, the avalanche exponents, α and τ, together with the spatial avalanche diffusion, z, provide a complete mapping to the DP universality class.

At peak susceptibility/intermediate arousal, burst avalanches exhibited power-law duration and size distributions with exponents $\alpha = 1.46 \pm 0.02$ [Fig. 2(a), blue circles] and $\tau = 1.27 \pm 0.01$ [Fig. 2(b) blue circles], estimated via nonlinear maximum likelihood [39]. These values quantitatively match 2+1-dimensional DP, for which $\tau_{\mathrm{DP}} = 1.268$ and $\alpha_{\mathrm{DP}} = 1.45$ (Fig. 2, black lines) [37]. To exclude alternative heavy-tailed distributions, we compared power-law and lognormal fits via the Akaike information criterion (AIC) [39]. Both size and duration yielded $\mathrm{AIC_{pl}}/\mathrm{AIC_{lgn}} < 0.5$, supporting the power-law fit.

In contrast, low arousal produced rapidly decaying size distributions and truncated durations [Figs. 2(a) and 2(b), red triangles], whereas high arousal produced cutoff distributions reflecting network-wide saturation [Figs. 2(a) and 2(b), green squares].

A stricter test of universality is the size-duration scaling relation $\langle S|T\rangle \sim T^{\gamma}$, where $\gamma = \frac{\alpha-1}{\tau-1}$ following from the size exponent relation $\tau = \frac{\gamma+\alpha-1}{\gamma}$. Contrasting the scaling plots over the three regimes, we found that intermediate arousal exhibited supralinear scaling $\langle S(T)\rangle \sim T^{1.7}$ with $\gamma = 1.70 \pm 0.05$ (inverse-variance weighted regression in log-log space) over multiple orders of magnitude [Fig. 2(c), blue circles] in close agreement with both the scaling exponent relationship, $\frac{1.46-1}{1.27-1} \approx 1.7$ and 2+1-dimensional DP [$\gamma_{\mathrm{DP}} = 1.68$; Fig. 2(c), dark line]. Low arousal preserved supralinear scaling, albeit only over an order of magnitude [Fig. 2(c), red triangles], while high arousal transitioned from supralinear to linear scaling, $\langle S(T)\rangle \sim T^{1}$, reflecting premature cessation from network-wide refractoriness [Fig. 2(c), green squares].

As our analysis tracks spatiotemporally contiguous cascades, we can also test spatial spreading statistics, which are rarely tested for in neural systems. Intermediate arousal displayed superdiffusive anomalous diffusion $R^2(t) \sim T^{z}$ with $z = 1.14 \pm 0.03$ [Fig. 2(d)], estimated via inverse-variance weighted regression in log-log space, matching the 2+1 DP diffusion $z_{\mathrm{DP}} = 1.1325$. In contrast, both low and high arousal exhibited linear diffusion ($z \approx 1$). Together, intermediate arousal uniquely satisfies the full hyperscaling set of exponents (α, τ, z), that defines the 2+1 DP universality class.

C. Universal avalanche shape collapse

While power-law distributions and scaling relations are essential indicators of criticality, self-similarity of avalanche temporal profiles provides the strongest evidence of criticality [40]. Let $\langle n(t|T)\rangle$ denote the average number of active sites at time at time t within avalanches of duration T. Under the scaling ansatz,

$$\langle n(t|T)\rangle = T^{\gamma-1}\mathcal{B}\left(\frac{t}{T}\right), \tag{13}$$

all avalanche profiles collapse onto a universal function $\mathcal{B}$ when properly rescaled. Rescaling using the DP predicted scaling $T^{1-\gamma_{\mathrm{DP}}}\langle n(t|T)\rangle$ against $\frac{t}{T}$ yielded a broad collapse at intermediate arousal (Fig. 3, blue), but not low (Fig. 3, red) or high arousal (Fig. 3, green). Optimal collapse, determined by minimizing range-normalized mean-variance [41], occurred at $\gamma = 1.72 \pm 0.05$, consistent with both exponent scaling and DP theory. Low arousal required larger renormalization ($\gamma = 2.78 \pm 0.05$), while high arousal failed to yield a global minimization, instead displaying two minima centered at $\gamma \sim 1.7$ and $\gamma \sim 4$, likely reflecting local and global avalanches. Universal burst profiles $\mathcal{B}$ were left-skewed, with intermediate arousal showing more symmetry (Fig. 3, black lines).

Taken together, only at intermediate arousal, where susceptibility peaks, do burst avalanches satisfy all hallmarks of directed percolation criticality: power-law size and duration distributions, scaling relations, hyperscaling, anomalous diffusion, and universal shape collapse. These results establish arousal-controlled bursting as a physiologically grounded control parameter that tunes cortical networks to a nonequilibrium phase transition in the 2+1 DP universality class.

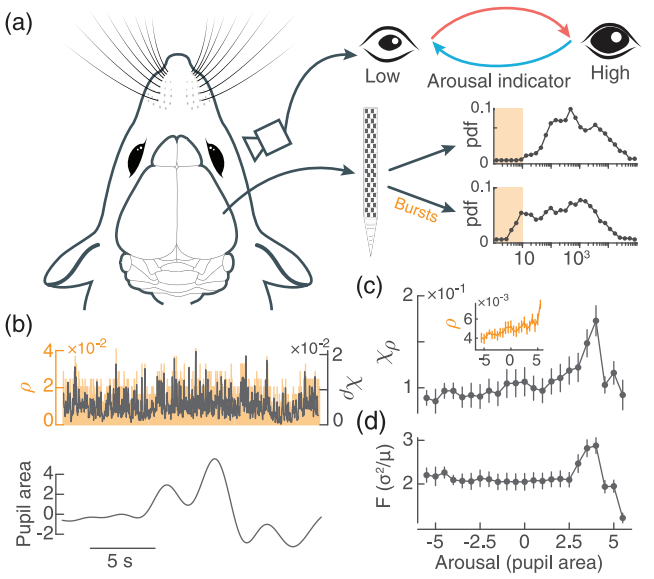

FIG. 4. Time-varying susceptibility fluctuates with pupil-inferred arousal *in vivo,* matching theoretical predictions. (a) Reanalysis of extracellular recordings of bursting neurons and nonluminance pupil fluctuations. (b) (Top) Instantaneous burst density (orange) and susceptibility (gray), along with (bottom) pupil area. (c) Instantaneous susceptibility (gray) as a function of pupil area showing a peak at intermediate-to-high arousal [contrast with Fig. 1(d)]. Inset: Burst density (yellow) against pupil area, increasing monotonically. (d) Burst-count Fano factor (σ^2/μ) against pupil area. Error bars are 95% CI.

D. Time-resolved susceptibility tracks arousal in vivo

The theory demonstrated here predicts that neuronal DP criticality depends on arousal state, yet most empirical studies are conducted under artificial neuromodulatory conditions (e.g., anesthesia, slice preparations) or during unconstrained fluctuations in arousal (awake behavior). Both conditions can obscure criticality signals, unless arousal is explicitly tracked. Here we overcome these limitations and test the model predictions by reanalyzing extracellular recordings from an awake mouse [42], isolating bursting neurons (using a standard definition of cells displaying an interspike interval < 10 ms; resulting in $n = 289$ cells) together with simultaneous pupillometry, a standard proxy of arousal dynamics [Fig. 4(a)].

Using short temporal windows (20 ms, $\Delta t = 1$ ms; results were robust for coarser windows up to 500 ms), we tracked simultaneous burst density [ρ; Fig. 4(b) top, orange], susceptibility [χ_ρ; Fig. 4(b) top, gray], and normalized pupil area [Fig. 4(b) bottom, gray]. Importantly, instantaneous susceptibility followed an inverted-U profile across arousal [Fig. 4(c)], peaking at intermediate-to-high arousal as predicted by our model. Mean burst rate [Fig. 4(c) inset] increased monotonically with pupil area ($r_s = 0.9$, $p = 3.3 \times 10^{-6}$; Spearman rank correlation), in contrast to a Poisson mechanism, which would predict a monotonic susceptibility and not the observed bump. Consistent with this dissociation, the burst-count Fano

factor (σ^2/μ) [43] retained the inverted-U profile against pupil area [Fig. 4(d)], ruling out an arousal-modulated Poisson explanation of the susceptibility peak.

IV. DISCUSSION

This proof-of-principle analysis confirms that signatures of criticality vary with arousal and demonstrates that unaccounted arousal fluctuations can obscure the determination of criticality across experiments and preparations. More broadly, these methodological implications establish high-temporal-resolution arousal tracking as a key requirement for future *in vivo* tests of neural criticality (e.g., using time-varying susceptibility or other recent dynamical approaches [44,45]).

We have identified arousal as a mechanistic control parameter that tunes cortical networks to nonequilibrium criticality within the universality class of directed percolation. In a physiologically grounded model of bursting neurons, an intermediate arousal regime exhibited peaked susceptibility, power-law avalanche size and duration distributions, hyperscaling, anomalous diffusion, and universal avalanche shape collapse, together comprising a complete characterization of 2+1 DP universality. Crucially, these results were only accessible by tracking spatiotemporally causal avalanches, rather than collapsing activity across time as is typical in empirical studies [36,46,47]. We outline a complete set of DP derived spatiotemporal avalanche exponents (α, τ, z) and time-resolved susceptibility predictions for future experimental validation.

Our findings offer a unifying mechanistic account of how arousal regulates neural susceptibility and information processing capacity. They indicate that cortical networks display criticality not at a fixed operating point [6], but flexibly through arousal tuning, consistent with neuromodulatory control. Peaked susceptibility at intermediate arousal provides a potential statistical-physics basis for the classic Yerkes-Dodson inverted-U relationship between arousal and behavioral performance [19,20].

More broadly, these results provide a resolution to the long-standing inconsistency in reported criticality across species, states, and recording methodologies. We propose that this inconsistency arises from variability in neuromodulatory tone. Empirical recordings under nonstationary, naturally fluctuating or pharmacologically altered arousal will inevitably mix subcritical, critical, and supercritical regimes, obscuring critical signatures. Our findings thus underscore that arousal must be treated as a key experimental control parameter rather than a confounding noise factor.

Together, these results bridge cellular biophysics, nonequilibrium statistical mechanics, and systems neuroscience by identifying a physiological mechanism—arousal-gated bursting—that tunes the brain through directed percolation criticality resolving the functional trade-off between dynamical regimes via adaptive neuromodulatory control.

ACKNOWLEDGMENTS

B.R.M was supported by the Australian Research Council's Discovery Early Career Researcher Award (DE260101935) and a Dementia Australia Research Foundation Project Grant. E.J.M. was supported by the Australian Research Council's Discovery Early Career Researcher Award (DE250100540). J.M.S was supported by the NHMRC Leadership Fellowship (2933162).

DATA AVAILABILITY

The data and model that support the findings of this article are openly available [48].

[1] L. Cocchi, L. L. Gollo, A. Zalesky, and M. Breakspear, Criticality in the brain: A synthesis of neurobiology, models and cognition, Prog. Neurobiol. **158**, 132 (2017).

[2] J. M. Beggs and D. Plenz, Neuronal avalanches in neocortical circuits, J. Neurosci. **23**, 11167 (2003).

[3] N. Friedman, S. Ito, B. A. W. Brinkman, M. Shimono, R. E. L. DeVille, K. A. Dahmen, J. M. Beggs, and T. C. Butler, Universal critical dynamics in high resolution neuronal avalanche data, Phys. Rev. Lett. **108**, 208102 (2012).

[4] T. Petermann, T. C. Thiagarajan, M. A. Lebedev, M. A. L. Nicolelis, D. R. Chialvo, and D. Plenz, Spontaneous cortical activity in awake monkeys composed of neuronal avalanches, Proc. Natl. Acad. Sci. USA **106**, 15921 (2009).

[5] B. R. Munn, E. J. Müller, I. Favre-Bulle, E. Scott, J. T. Lizier, M. Breakspear, and J. M. Shine, Multiscale organization of neuronal activity unifies scale-dependent theories of brain function, Cell **187**, 7303 (2024).

[6] K. B. Hengen and W. L. Shew, Is criticality a unified setpoint of brain function? Neuron **113**, 2582 (2025).

[7] A. J. Fontenele, N. A. P. De Vasconcelos, T. Feliciano, L. A. A. Aguiar, C. Soares-Cunha, B. Coimbra, L. Dalla Porta, S. Ribeiro, A. J. Rodrigues, N. Sousa, P. V. Carelli, and M. Copelli, Criticality between cortical states, Phys. Rev. Lett. **122**, 208101 (2019).

[8] E. J. Müller, B. R. Munn, and J. M. Shine, The brain that controls itself, Curr. Opin. Behav. Sci. **63**, 101499 (2025).

[9] C. V. Stewart and D. Plenz, Inverted-U profile of dopamine–NMDA-mediated spontaneous avalanche recurrence in superficial layers of rat prefrontal cortex, J. Neurosci. **26**, 8148 (2006).

[10] B. R. Munn, E. J. Müller, G. Wainstein, and J. M. Shine, The ascending arousal system shapes neural dynamics to mediate awareness of cognitive states, Nat. Commun. **12**, 6016 (2021).

[11] J. M. Shine, Neuromodulatory control of complex adaptive dynamics in the brain, Interface Focus. **13**, 20220079 (2023).

[12] W. L. Shew, H. Yang, S. Yu, R. Roy, and D. Plenz, Information capacity and transmission are maximized in balanced cortical networks with neuronal avalanches, J. Neurosci. **31**, 55 (2011).

[13] O. Kinouchi and M. Copelli, Optimal dynamical range of excitable networks at criticality, Nature Phys. **2**, 348 (2006).

[14] L. L. Gollo, Coexistence of critical sensitivity and subcriticality specificity can yield optimal population coding, J. R. Soc. Interface **14**, 20170207 (2017).

[15] W. P. Clawson, N. C. Wright, R. Wessel, and W. L. Shew, Adaptation towards scale-free dynamics improves cortical stimulus discrimination at the cost of reduced detection, PLoS Comput. Biol. **13**, e1005574 (2017).

[16] T. L. Ribeiro, M. Copelli, F. Caixeta, H. Belchior, D. R. Chialvo, M. A. L. Nicolelis, and S. Ribeiro, Spike avalanches exhibit universal dynamics across the sleep-wake cycle, PLoS One **5**, e14129 (2010).

[17] C. Huo, F. Lombardi, C. Blanco-Centurion, P. J. Shiromani, and P. Ch. Ivanov, Role of the locus coeruleus arousal promoting neurons in maintaining brain criticality across the sleep–wake cycle, J. Neurosci. **44**, e1939232024 (2024).

[18] W. L. Shew, W. P. Clawson, J. Pobst, Y. Karimipanah, N. C. Wright, and R. Wessel, Adaptation to sensory input tunes visual cortex to criticality, Nature Phys. **11**, 659 (2015).

[19] G. Aston-Jones and J. D. Cohen, An integrative theory of locus coeruleus-norepinephrine function: Adaptive gain and optimal performance, Annu. Rev. Neurosci. **28**, 403 (2005).

[20] R. M. Yerkes and J. D. Dodson, The relation of strength of stimulus to rapidity of habit-formation, J. Comp. Neurol. Psychol. **18**, 459 (1908).

[21] L. Papadopoulos, S. Jo, K. Zumwalt, M. Wehr, S. Jaramillo, D. A. McCormick, and L. Mazzucato, Modulation of metastable ensemble dynamics explains the inverted-U relationship between tone discriminability and arousal in auditory cortex, Neuron **114**, 740 (2026).

[22] L. Beerendonk, J. F. Mejías, S. A. Nuiten, J. W. De Gee, J. J. Fahrenfort, and S. Van Gaal, A disinhibitory circuit mechanism explains a general principle of peak performance during mid-level arousal, Proc. Natl. Acad. Sci. USA **121**, e2312898121 (2024).

[23] M. Suzuki and M. E. Larkum, General anesthesia decouples cortical pyramidal neurons, Cell **180**, 666 (2020).

[24] E. M. Izhikevich, N. S. Desai, E. C. Walcott, and F. C. Hoppensteadt, Bursts as a unit of neural information: Selective communication via resonance, Trends Neurosci. **26**, 161 (2003).

[25] J. Aru, M. Suzuki, and M. E. Larkum, Cellular mechanisms of conscious processing, Trends Cogn. Sci. **24**, 814 (2020).

[26] H. Hinrichsen, Non-equilibrium critical phenomena and phase transitions into absorbing states, Adv. Phys. **49**, 815 (2000).

[27] S. di Santo, P. Villegas, R. Burioni, and M. A. Muñoz, Simple unified view of branching process statistics: Random walks in balanced logarithmic potentials, Phys. Rev. E **95**, 032115 (2017).

[28] T. T. A. Carvalho, A. J. Fontenele, M. Girardi-Schappo, T. Feliciano, L. A. A. Aguiar, T. P. L. Silva, N. A. P. De Vasconcelos, P. V. Carelli, and M. Copelli, Subsampled directed-percolation models explain scaling relations experimentally observed in the brain, Front. Neural Circuits **14**, 576727 (2021).

[29] M. Girardi-Schappo, E. F. Galera, T. T. A. Carvalho, L. Brochini, N. L. Kamiji, A. C. Roque, and O. Kinouchi, A unified theory of E/I synaptic balance, quasicritical neuronal avalanches and asynchronous irregular spiking, J. Phys. Complex. **2**, 045001 (2021).

[30] B. R. Munn, E. J. Müller, V. Medel, S. L. Naismith, J. T. Lizier, R. D. Sanders, and J. M. Shine, Neuronal connected burst cascades bridge macroscale adaptive signatures across arousal states, Nat. Commun. **14**, 6846 (2023).

[31] B. R. Munn, E. J. Müller, J. Aru, C. J. Whyte, A. Gidon, M. E. Larkum, and J. M. Shine, A thalamocortical substrate for integrated information via critical synchronous bursting, Proc. Natl. Acad. Sci. USA **120**, e2308670120 (2023).

[32] C. J. Whyte, E. J. Müller, J. Aru, M. Larkum, Y. John, B. R. Munn, and J. M. Shine, A burst-dependent thalamocortical substrate for perceptual awareness, PLoS Comput. Biol. **21**, e1012951 (2025).

[33] E. M. Izhikevich, Simple model of spiking neurons, IEEE Trans. Neural Netw. **14**, 1569 (2003).

[34] K. Kang, M. Shelley, and H. Sompolinsky, Mexican hats and pinwheels in visual cortex, Proc. Natl. Acad. Sci. USA **100**, 2848 (2003).

[35] R. V. Williams-García, M. Moore, J. M. Beggs, and G. Ortiz, Quasicritical brain dynamics on a nonequilibrium Widom line, Phys. Rev. E **90**, 062714 (2014).

[36] E. Tagliazucchi, P. Balenzuela, D. Fraiman, and D. R. Chialvo, Criticality in large-scale brain FMRI dynamics unveiled by a novel point process analysis, Front. Physiol. **3**, 15 (2012).

[37] M. A. Muñoz, R. Dickman, A. Vespignani, and S. Zapperi, Avalanche and spreading exponents in systems with absorbing states, Phys. Rev. E **59**, 6175 (1999).

[38] K.-E. Lee, M. A. Lopes, J. F. F. Mendes, and A. V. Goltsev, Critical phenomena and noise-induced phase transitions in neuronal networks, Phys. Rev. E **89**, 012701 (2014).

[39] A. Clauset, C. R. Shalizi, and M. E. J. Newman, Power-law distributions in empirical data, SIAM Rev. **51**, 661 (2009).

[40] J. P. Sethna, K. A. Dahmen, and C. R. Myers, Crackling noise, Nature (London) **410**, 242 (2001).

[41] N. Marshall, N. M. Timme, N. Bennett, M. Ripp, E. Lautzenhiser, and J. M. Beggs, Analysis of power laws, shape collapses, and neural complexity: New techniques and MATLAB support via the NCC toolbox, Front. Physiol. **7**, (2016).

[42] C. Stringer, M. Pachitariu, N. Steinmetz, C. B. Reddy, M. Carandini, and K. D. Harris, Spontaneous behaviors drive multidimensional, brainwide activity, Science **364**, 6437 (2019).

[43] B. Munn, N. Zeater, A. N. Pietersen, S. G. Solomon, S. K. Cheong, P. R. Martin, and P. Gong, Fractal spike dynamics and neuronal coupling in the primate visual system, J. Physiol. **598**, 1551 (2020).

[44] J. S. Sooter, A. J. Fontenele, A. K. Barreiro, C. Ly, K. B. Hengen, and W. L. Shew, Defining and measuring proximity to criticality, bioRxiv (2025).

[45] B. Harris, L. L. Gollo, and B. D. Fulcher, Tracking the distance to criticality in systems with unknown noise, Phys. Rev. X **14**, 031021 (2024).

[46] B. Munn and P. Gong, Critical dynamics of natural time-varying images, Phys. Rev. Lett. **121**, 058101 (2018).

[47] A. Ponce-Alvarez, A. Jouary, M. Privat, G. Deco, and G. Sumbre, Whole-brain neuronal activity displays crackling noise dynamics, Neuron **100**, 1446 (2018).

[48] https://github.com/Bmunn/Layer5_Arousal.